Mg–Al layered double hydroxide intercalated with $[Ni(edta)]^{2-}$ chelate as a precursor for an efficient catalyst of methane reforming with carbon dioxide

Andrey I. Tsyganok *, Kunio Suzuki, Satoshi Hamakawa, Katsuomi Takehira [a] and Takashi Hayakawa *

National Institute of Advanced Industrial Science and Technology, Institute for Materials and Chemical Process, Tsukuba Central 5, Higashi 1-1-1, Tsukuba 305-8565, Japan

E-mail: atsygano@nimc.go.jp; t.hayakawa@aist.go.jp

[a] *Department of Applied Chemistry, Hiroshima University, Kagamiyama 1-4-1, Higashi-Hiroshima 739-8527, Japan*

Received 18 May 2001; accepted 10 August 2001

Coprecipitation of Mg^{2+} and Al^{3+} with pre-synthesized $[Ni(edta)]^{2-}$ chelate at basic pH resulted in formation of a new layered double hydroxide (LDH) where $[Ni(edta)]^{2-}$ species occupied the interlayer space. The synthesized LDH was characterized by X-ray powder diffraction, diffuse reflectance FTIR and thermogravimetry-differential thermal analysis under inert and oxidative atmosphere. Calcination of LDH led to NiMgAl mixed oxide which after reduction with hydrogen exhibited high catalytic function toward the reaction of methane reforming with carbon dioxide to synthesis gas. The catalyst maintained high activity within 150 h time on stream at 800 °C and could be used repeatedly after regeneration. Although coke deposition onto the catalyst surface attained 5–10 wt%, it did not diminish reagent conversion and product selectivity.

KEY WORDS: methane; dry reforming; nickel; layered double hydroxides; intercalation

1. Introduction

The reaction of methane reforming with carbon dioxide (also referred to as *dry reforming of methane*, DRM) is not only of commercial interest, as it gives rise to synthesis gas, but also of environmental concern: it employs methane and carbon dioxide, two main components of greenhouse gases, and therefore leads to the reduction of their emission to the atmosphere. The reaction is usually catalyzed by supported noble metals or Ni-based catalysts that are more cost-effective [1]. Nickel can be introduced *via* common impregnation technique [2], sol–gel method [3,4] or by obtaining a Ni-containing solid solution [5–10]. Nickel-based catalysts can be also prepared *via* a hydrotalcite-like precursor when Ni^{2+}, Mg^{2+} and Al^{3+} are precipitated at basic pH with carbonate anion [11]. It leads to the formation of LDH phase with a layered structure very similar to that of hydrotalcite [12].

We have recently reported that incorporation of nickel into Mg–Al LDH can be performed by an alternative approach. It was based on the ability of Ni^{2+} to react with an anionic chelating agent of $edta^{4-}$, *i.e.*, ethylenediaminetetraacetate, forming the highly stable $[Ni(edta)]^{2-}$ species (denoted hereafter by NiY^{2-}). It was suggested that coprecipitation of Mg^{2+} and Al^{3+} with pre-formed NiY^{2-} gave rise to Mg–Al LDH intercalated with Ni chelate [13]. However, the thorough characterization of the newly synthesized phase (MgAl–NiY) had not been done so far and was highly desired.

In this work we present the details of MgAl–NiY synthesis as well as the experimental data confirming involvement of nickel into Mg–Al LDH structure as chelated NiY^{2-} species. The reductively pretreated NiMgAl mixed oxide, which was derived from such LDH, demonstrated high activity and sustainability toward DRM reaction to synthesis gas. Moreover, the coke deposition process and morphology of catalytically produced carbon deposits will be discussed.

2. Experimental

2.1. Reagents and materials

The reagents used in this study were purchased from Wako Chemicals Co. All chemicals had 98–99% purity and were used without additional purification treatment. The distilled and deionized water was used throughout the work. The reference materials included synthetic hydrotalcite (*i.e.*, $[Mg_6Al_2(OH)_{16}]CO_3$) and $[NiMg_5Al_2(OH)_{16}]CO_3$ LDH (designated as $MgAl–CO_3$ and $NiMgAl–CO_3$, respectively), disodium nickel(II) ethylenediaminetetraacetate dihydrate $Na_2Ni(edta)\cdot 2H_2O$ (denoted hereafter by Na_2NiY), magnesium oxide powder (0.1 μm particle size) of 99.9% purity, and a physical mixture of Na_2NiY with MgO. In order to prepare the physical mixture, the powders were placed in a screw-cap vial of 20 cm^3 capacity that was further horizontally rotated with 100 rpm speed at room temperature for 24 h.

* To whom correspondence should be addressed.

1011-372X/01/1100-0075$19.50/0

2.2. Synthesis of LDH

The synthesis of Mg–Al double hydroxide included two steps. First, an aqueous solution of NiY^{2-} was prepared at room temperature. It was done by dropwise addition of Ni(II) nitrate solution (100 mmol in 100 cm^3 of water) to tetrasodium salt of edta (100 mmol) dissolved in 100 cm^3 of water. The obtained deep blue solution of NiY^{2-} was transferred into a three-neck reaction flask equipped with a magnet stirrer and kept at 63 °C. The second step of LDH synthesis included dropwise addition of 100 cm^3 aqueous solution of Mg(II) and Al(III) nitrates (30 and 10 mmol, respectively) to NiY^{2-} at pH = 10.5 which was adjusted by addition of aqueous 1.0 M solution of NaOH. When the solution of metal cations was entirely added, the obtained pale-blue slurry was stirred at 63 °C for 1 h, followed by 18 h aging without stirring at the same temperature. The resultant precipitate was separated by filtration, washed with distilled and deionized water until the filtrate was free from NiY^{2-} ions, dried in air at 80 °C for 16 h and kept in a desiccator under vacuum at room temperature.

Calcination of the synthesized solid at 500 °C for 16 h in air yielded the light green NiMgAl mixed oxide that was further used as a catalyst.

2.3. Characterization techniques

X-ray diffraction patterns (XRD) of powder samples were recorded at room temperature under air using a MacScience MXP18 diffractometer with Cu Kα irradiation source (λ 1.54056 Å) at 40 kV voltage and 50 mA current.

Thermogravimetry and differential thermal analysis (TG-DTA) were carried out under inert (20 $cm^3\,min^{-1}$ of N_2) and oxidative (20 $cm^3\,min^{-1}$ of air) atmosphere with TGA-50 and DTA-50 analyzers (both from Shimadzu, Co.) using 30–50 mg of sample and 5.0 °C min^{-1} temperature rate.

Specific surface area of NiMgAl mixed oxide was measured by adsorption of N_2 at liquid nitrogen temperature using a Shimadzu Micromeritics FlowSorb II 2300 analyzer with N_2 : He (33 : 67 by volume) gas mixture. The powdered sample (30–35 mg) was degassed at 100 °C for 1 h and then cooled to room temperature before area measurement. After several adsorption–desorption cycles an average value of 115.7 $m^2\,g^{-1}$ was obtained by BET method.

The elemental composition of NiMgAl mixed oxide was determined by using an inductively coupled plasma emission spectrometer (ICP-ES) of Thermo Jarrel-Ash IRIS/AP model. The mixed oxide was first dissolved in a small volume of concentrated nitric acid and then diluted by water to the concentration level suitable for ICP-ES measurements. It was found that the mixed oxide had a formula of $NiMg_7Al_2O_{11}$ which corresponded to a nickel content of 10 at%.

Scanning electron microscopy (SEM) studies were performed using a Hitachi S-800 apparatus with 15 kV accelerating voltage. Transmission electron microscopy (TEM) was done with a Jeol JEM-2010F machine equipped with a Gatan slow-scan camera for high-resolution observation. The accelerating voltage applied was 200 kV. Specimens for SEM and TEM were prepared by standard techniques.

Diffuse reflectance Fourier transform infrared (DRIFT) spectra were recorded with a Nicolet Magna-IR 750 spectrometer equipped with a chamber for DRIFT measurements, a KBr beam splitter, DTGS (KBr) detector, and He–Ne laser (λ 633 nm). A chamber with powdered sample was purged with nitrogen (40 $cm^3\,min^{-1}$) for 30 min prior to every DRIFT measurement. Data acquisition for each sample involved 200 scans taken within 4 min with 4 cm^{-1} resolution at room temperature under nitrogen flow.

2.4. Catalytic activity tests

NiMgAl mixed oxide prepared from MgAl–NiY LDH was pressed into a tablet and ground up to sieve 212–425 μm fraction of particles that was used for catalytic experiments. The catalyst (150 mg) was well mixed with Wakogel silica G (250 mg; 300–600 μm) and C-100 (250 mg; 150–425 μm). The vertically mounted quartz tube reactor (8 mm i.d.) was charged with a mixture of catalyst and silica, and gases were introduced with upstream flow direction. Activation of the Ni catalyst involved the reductive treatment with hydrogen ($H_2 : N_2$ 10 : 35 $cm^3\,min^{-1}$) at 600 °C for 15 min, followed by cooling to room temperature under pure nitrogen. Then the reactor was fed with the reagent gas mixture of $CH_4 : CO_2 : N_2$ (25 : 25 : 35 $cm^3\,min^{-1}$) and heated with 5.0 °C min^{-1} rate to the desired temperature. When the reactor temperature reached the stated value, the sampling of post-reactor gas phase was started. Analysis of reaction products was done by gas chromatography using Porapak Q and molecular sieve 5A packed columns. After 6 h time on stream the admission of methane and carbon dioxide was stopped, and the reactor was cooled to room temperature under a flow of nitrogen.

2.5. Temperature-programmed oxidation of deposited coke

To evaluate the amount of catalytically produced coke, the spent catalyst was subjected to temperature-programmed oxidation (TPO) from room temperature to 850 °C with 2.5 °C min^{-1} rate under 40 $cm^3\,min^{-1}$ flow of air. Monitoring of CO_2 emission was carried out with 10 min intervals (*i.e.*, by 25 °C steps) by gas chromatography. The total amount of deposited carbon was calculated from the quantity of CO_2 released during the TPO experiment.

3. Results and discussion

3.1. Characterization of catalyst precursor

The results of powder XRD measurements are shown in figure 1. It can be readily seen that the diffractogram of MgAl–NiY (pattern A) has a specific set of reflection peaks that significantly differs from those of reference materials. The precise measurements of the present three symmetric

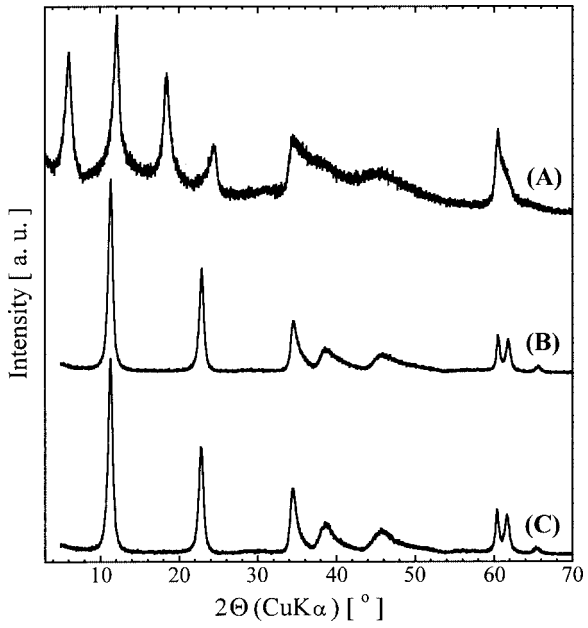

Figure 1. X-ray powder diffraction patterns of Mg–Al double hydroxides: (A) MgAl–NiY, (B) NiMgAl–CO_3 and (C) MgAl–CO_3 (hydrotalcite).

Table 1
Supplementary XRD data for MgAl–NiY and reference LDHs.

	MgAl–NiY	NiMgAl–CO_3	MgAl–CO_3
d_{003} (Å)	14.72	7.80	7.82
2θ (°)	6.0	11.34	11.30
Intensity (cps)	1983	6850	6119
FWHM	0.44	0.40	0.44
d_{006} (Å)	7.31	3.89	3.90
2θ (°)	12.10	22.86	22.78
Intensity (cps)	2422	3758	3406
FWHM	0.42	0.40	0.42
d_{009} (Å)	4.83	2.60	2.60
2θ (°)	18.36	34.46	34.44
Intensity (cps)	1726	1920	2138
FWHM	0.44	0.58	0.64
d_{110} (Å)	1.53	1.53	1.53
2θ (°)	60.56	60.52	60.42
Intensity (cps)	1118	1412	1463
FWHM	0.40	0.38	0.32
Cell parameters (Å)			
a	3.06	3.06	3.06
c	43.83	23.38	23.42

peaks at 2θ 6.0°, 12.10° and 18.36° revealed basal spacings *d* of 14.7, 7.3 (as $d/2$) and 4.8 Å (as $d/3$). These results indicated that the newly synthesized double hydroxide phase had a layered structure (table 1). Furthermore, the subtraction of 4.8 Å as an average brucite sheet thickness from the *d* value gave 9.9 Å for the interlayer distance that could be attributed to intercalation of the NiY^{2-} chelate. In contrast, when Ni^{2+} was coprecipitated with Mg^{2+} and Al^{3+} cations, the resulting NiMgAl–CO_3 LDH demonstrated an XRD pattern very similar to that of hydrotalcite, which can be readily seen from the comparison of B and C patterns in figure 1 and from data in table 1. The fact that all three LDH samples showed reflection peaks near 2θ 60° and therefore the same d_{110} value (1.53 Å) indicated that no change in the average cation–cation distance in the brucite-like layers had occurred. As a result, the cell parameter *a* calculated as $2d_{110}$ gave a value of 3.06 Å for all LDH samples which was consistent with [12]. Assuming that all three LDH phases crystallize with rhombohedral 3R packing of layers allows calculating the cell parameter *c* [14,15]. As it can be seen in table 1, a *c* value of 43.83 Å was obtained for MgAl–NiY LDH whereas it was about 23.4 Å for NiMgAl–CO_3 and MgAl–CO_3. Thus, intercalation of NiY^{2-} species between brucite sheets of Mg–Al LDH led to expansion of *d* spacing and consequently an increase in cell parameter *c*.

It is well known that Mg–Al LDHs are highly capable to absorb CO_2 from air to form the hydrotalcite-like carbonate phase. Therefore, significant care should be taken for the synthesis of carbonate-free LDH phase. In our studies, all steps of the MgAl–NiY synthesis (*i.e.*, coprecipitation of Mg^{2+} and Al^{3+} with NiY^{2-}, aging of LDH precipitate, its filtration and drying) were carried out under air. However, it did not cause formation of an XRD-detectable carbonate phase because no impurity peaks related to hydrotalcite phase were observed in the XRD pattern of MgAl–NiY LDH. In our opinion, it was mostly due to use of the degassed and deionized water as a solvent and a high starting concentration of NiY^{2-} ions in aqueous solution.

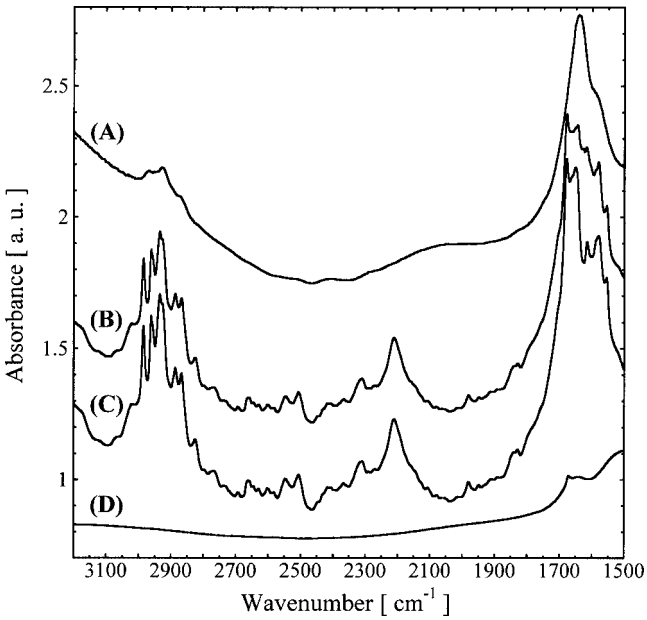

Figure 2. Diffuse reflectance FTIR spectra of (A) MgAl–NiY LDH, (B) physical mixture of Na_2NiY with MgO (1 : 7 by mol), (C) pure Na_2NiY and (D) pure MgO.

To confirm the hypothesis on formation of Mg–Al LDH intercalated with NiY^{2-} chelate species, diffuse reflectance FTIR spectroscopy was applied. The results obtained for MgAl–NiY and reference materials are shown in figure 2. Pure Na_2NiY and its physical mixture with MgO (shown as spectra C and B) demonstrated the characteristic ab-

Table 2
DRIFT results for MgAl–NiY and reference materials.

Material	Absorption bands (cm^{-1})	Band assignment
MgAl–NiY	1640	Stretching of $–COO^-$ groups coordinated to Ni(II);
	1588 (shoulder)	uncoordinated $–COO^-$ stretching
	2873, 2929, 2953, 2970	All peaks are due to antisymmetric and symmetric –C–H stretching of methylene groups
Physical mixture of Na_2NiY : MgO 1 : 7 (mol/mol)	1555, 1580, 1617, 1645, 1678	Antisymmetric stretching of coordinated and uncoordinated $–COO^-$ groups
	2868, 2887, 2935, 2962, 2986	Antisymmetric and symmetric –C–H stretching of methylene groups
Na_2NiY	1555, 1580, 1615, 1652, 1678	Antisymmetric stretching of coordinated and uncoordinated $–COO^-$ groups
	2868, 2887, 2935, 2962, 2986	Antisymmetric and symmetric –C–H stretching of methylene groups
MgO	1644, 1671	C=O stretching of CO_2 strongly adsorbed on MgO surface

sorption at wavenumbers of 2800–3050 cm^{-1} due to C–H stretching of methylene functions of Y^{4-} ligand as well as at the 1500–1700 cm^{-1} region that was characteristic of C=O vibrations of carboxylic groups. The presence of a notable broadened peak at 2212 cm^{-1} in spectra B and C indicated that the reference Na_2NiY and its mixture with MgO contained an impurity bearing a C≡N functional group. According to literature, H_4Y and its derivatives are commercially produced by two methods, both employing CN-containing chemicals [16]. The first method is a base-catalyzed condensation of ethylenediamine with formaldehyde and sodium cyanide that directly gives Y^{4-} and then H_4Y upon acidifying [17]. By another technique, condensation of ethylenediamine with formaldehyde and HCN gives with a high yield (ethylenedinitrilo)tetraacetonitrile $[(NCCH_2)_2NCH_2CH_2N(CH_2CN)_2]$ which is further hydrolyzed to Y^{4-} using sodium hydroxide solution [18]. In our studies, the starting reagents had purity higher than 98.0%. Moreover, synthesis of MgAl–NiY LDH was carried out in a hot aqueous solution at a moderately high basic pH. It seemed reasonable to assume that under such conditions any CN-containing impurity had been readily hydrolyzed. As a result, the DRIFT spectrum of MgAl–NiY LDH did not reveal absorption at 2200 cm^{-1} (see spectrum (A) in figure 2). The supplementary data on DRIFT bands assignment are presented in table 2. As NiY^{2-} chelate contains four COO^- functional groups, the resulting DRIFT spectrum of MgAl–NiY LDH showed strong absorption at 1640 cm^{-1} which was related to stretching of COO^- groups coordinated to Ni(II) [19]. The presence of a peak shoulder at 1588 cm^{-1} could be assigned to stretching of a free (*i.e.*, uncoordinated) COO^- group. In such a case Y^{4-} chelate behaved as a quinquedentate ligand occupying five coordination places of octahedral Ni^{2+}. The sixth place was captured by a water molecule [20]. Four broad but readily distinguishable peaks of low intensity at 2800–3000 cm^{-1} were due to C–H stretching of methylene groups of NiY^{2-} chelate [21]. Thus, the results of DRIFT studies clearly indicated that MgAl–NiY LDH contained the chelated Ni species that kept integrity and showed IR absorption behavior similar to that of free (*i.e.*, non-incorporated) NiY^{2-} species of Na_2NiY.

Figure 3 represents the results of TG-DTA studies performed under the inert (nitrogen) atmosphere with MgAl–NiY and reference materials at 5.0 °C min^{-1} temperature rate. As can be seen in figure 3, the main reduction in weight of MgAl–NiY, pure Na_2NiY and Na_2NiY–MgO mixture occurred at temperatures of 360–420 °C. As for MgO preliminarily exposed to indoor air for 5 days, its main loss in weight took place at lower temperature (300–360 °C). The DTA pattern of MgAl–NiY shown as curve (A*) in figure 3 presents two endothermic peaks. The broadened peak at 141 °C related to the desorption of physisorbed and structural water while the intensive one at 409 °C was assigned to (i) dehydroxylation of Mg–Al double hydroxide, (ii) collapse of the layered structure and (iii) thermal decomposition of entrapped NiY^{2-} species. Pure Na_2NiY (B*) and its mixture with MgO (C*) revealed DTA profiles very similar to each other. Both showed small endothermic peaks at 92–97 °C, which corresponded to the removal of physisorbed water, whereas higher temperature (225–233 °C) was needed for desorption of structural water. The peak at 395 °C with a shoulder at 406 °C for Na_2NiY and the poorly resolved peak doublet (395–407 °C) for the Na_2NiY–MgO mixture were due to thermal decomposition of NiY^{2-} species. Compared to all NiY^{2-}-containing samples, the air-pretreated MgO showed only one endothermic peak at 346 °C that was due to release of CO_2 strongly adsorbed by MgO from indoor air. Thermodesorption of water from MgO occurred at temperature lower than 240 °C (curve (D) in figure 3) and did not bring about a notable endothermic peak in the DTA profile (curve (D*)).

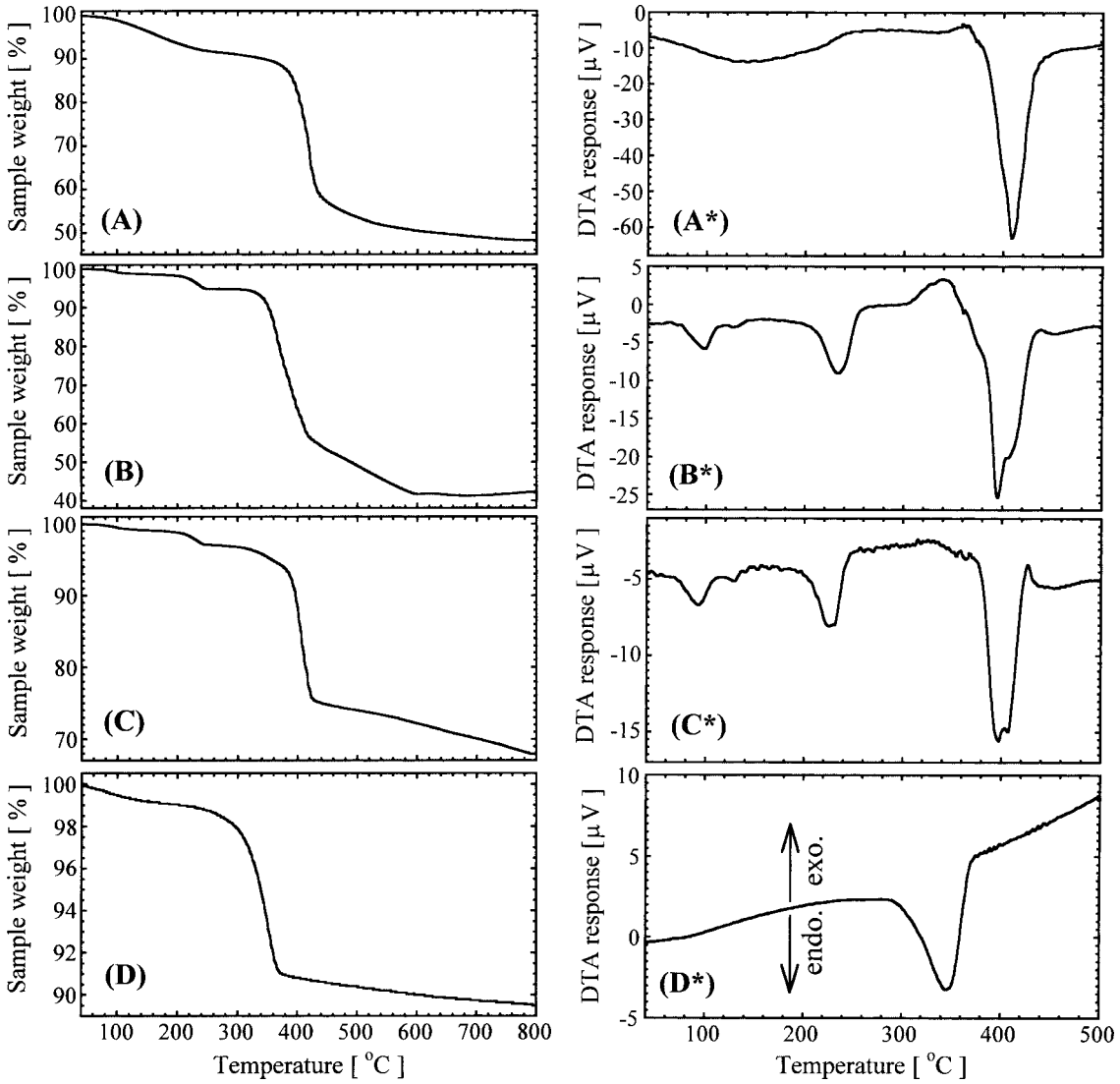

Figure 3. TG-DTA behavior of materials under nitrogen (20 $cm^3\,min^{-1}$) atmosphere: MgAl–NiY (A, A*), pure Na_2NiY (B, B*), physical mixture of Na_2NiY with MgO of 1 : 10 ratio by mol (C, C*), and MgO exposed to indoor air at room temperature for 5 days (D, D*).

The fact, that the NiY^{2-} species contains six methylene groups and two tertiary amines per every chelate anion, strongly suggested that the total oxidation process of the NiY^{2-} species must be an exothermic reaction, regardless of the spatial state of the NiY^{2-} chelate (*i.e.*, involved into the LDH structure as in MgAl–NiY or "free" as in Na_2NiY). In other words, the presence of sufficient organic content in any material due to NiY^{2-} species implied that under oxidative atmosphere the characteristic exothermic peak relating to the combustion of the Y^{4-} ligand ought to appear in the DTA profile. To verify this assumption, MgAl–NiY and reference samples were subjected to TG-DTA analysis under flow of air at 5.0 °C min^{-1} temperature rate. The results obtained are shown in figure 4. The first feature that can be seen from the comparison of TG profiles of MgAl–NiY, pure Na_2NiY and Na_2NiY–MgO mixture (curves A, B and C) is that the drastic decrease in sample weight occurred at temperature markedly less than 400 °C which significantly differed from TG curves obtained under nitrogen flow. The air-pretreated MgO (curve D) was the only material that revealed the same TG profile under air as that obtained under nitrogen.

The results of DTA analysis done under air strikingly differed from those obtained under nitrogen, too. As expected, all samples containing NiY^{2-} species exhibited intensive exothermic peaks that could definitely be attributed to the combustion of Y^{4-} ligand of NiY^{2-} chelate. Thus, two sharp peaks at 380 and 384 °C were recorded with MgAl–NiY (curve (A*) in figure 4) while the combustion of Y^{4-} of Na_2NiY led to appearance of a sharp peak at 368 °C and a main broad peak with maximum at 382 °C (B*). The interesting feature of DTA behavior of the Na_2NiY–MgO physical mixture is that the presence of MgO had a promoting effect on Y^{4-} combustion leading to a shift of DTA peak maximum to 364 °C (C*). Weak endothermic peaks at 97 and 230 °C in patterns (B*) and (C*) were due to release of physisorbed and structural water, respectively, as it took place under inert atmosphere (compare with curves (B*) and (C*) in figure 3). The air-pretreated MgO (D*) demonstrated

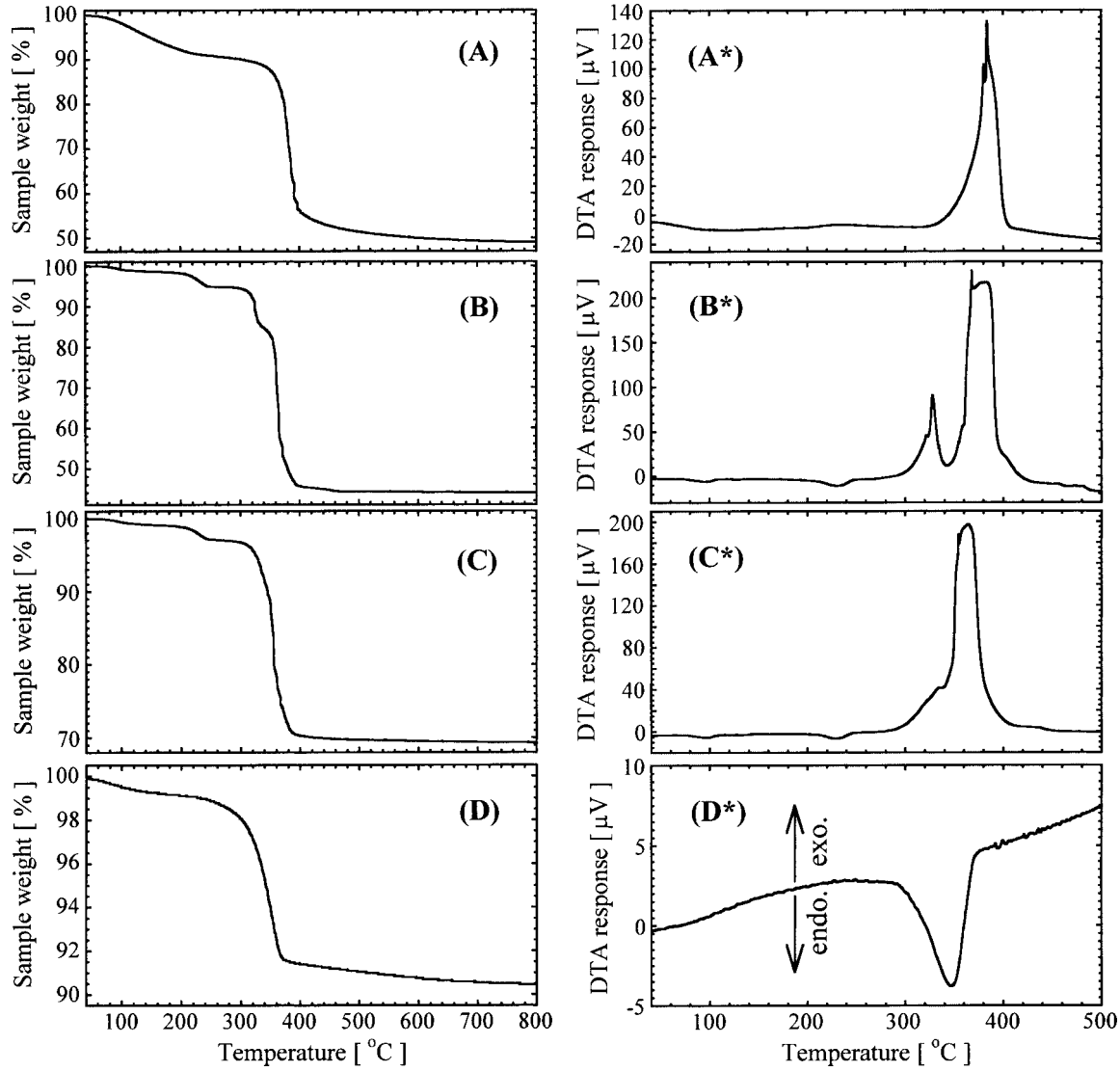

Figure 4. TG-DTA behavior of materials under air (20 $cm^3\ min^{-1}$): curves assignment is the same as in figure 3.

an independent behavior: the resultant DTA profile had an endothermic peak at 346 °C under both inert and oxidative atmosphere. In other words, desorption of CO_2 strongly bound to basic surface of magnesia was an endothermic reaction which did not depend on the atmosphere used in the TG-DTA studies.

Finally, the notable exothermic peak at 328 °C in the DTA profile of Na_2NiY (curve (B*) in figure 4) was most probably due to combustion of organic impurity of Na_2NiY. We believe it could be (ethylenedinitrilo)tetraacetonitrile, trace amount of which ought to offer a significant exothermic response of the DTA analyzer under oxidative atmosphere.

3.2. Ni-catalyzed reforming of methane with CO_2 at various temperatures

As reforming of methane with carbon dioxide to synthesis gas is an endothermic reaction, a rise in temperature improves conversion of CH_4 and CO_2. The results obtained at various temperatures with the Ni catalyst that was prepared from MgAl–NiY LDH are shown in figure 5. For every tested temperature CO_2 conversion was notably higher than that of CH_4. It was presumably due to the side reaction of reverse water gas shift (RWGS) which accompanied the target DRM reaction [1]. By this reason the selectivity to H_2 lowered to about 61% at 500 °C and to 91% at 600 °C. It should be pointed out that at all the tested temperatures the reductively pretreated Ni catalyst revealed a sustainable activity toward DRM reaction within 6 h of time on stream demonstrating no decrease in conversion and/or product selectivity. For instance, at 800 °C, conversion of CH_4 and CO_2 reached 95 and 98% with keeping product selectivity at 98% level for both H_2 and CO.

$$CO_2 + H_2 \rightleftharpoons CO + H_2O \quad \text{(RWGS)}$$

In order to measure the amount of coke that was deposited onto the catalyst surface, the spent catalysts were subjected to TPO. As can be seen in figure 6, the peak maximum of CO_2 emission (*i.e.*, the temperature at which the maximum

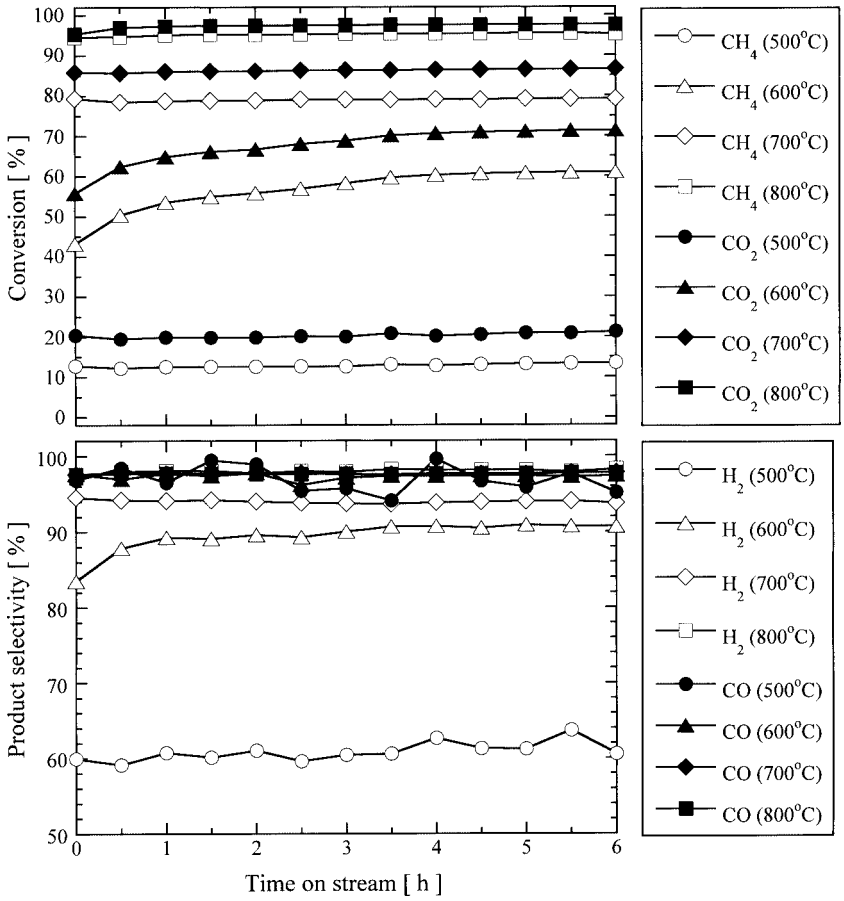

Figure 5. Nickel-catalyzed dry reforming of methane to synthesis gas at various temperatures.

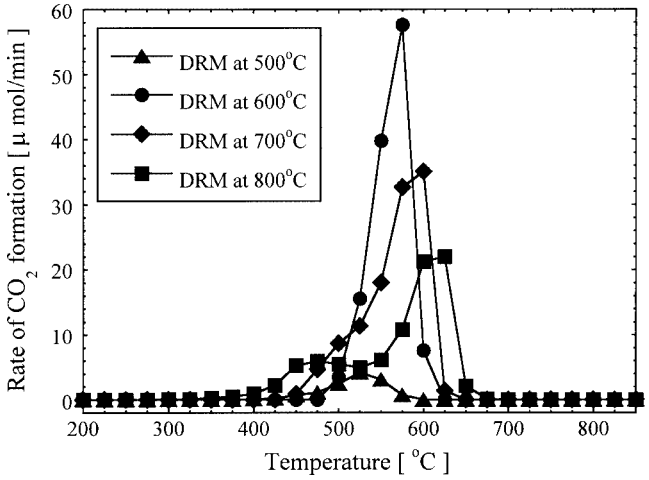

Figure 6. Temperature-programmed oxidation of coke deposited over Ni catalyst during DRM at various temperatures.

amount of CO_2 was released) correlated with the temperature at which DRM was performed. In other words, the coke deposited over the catalyst at higher DRM temperature required higher temperature for its oxidative removal. These results indicate that carbon deposits formed at various DRM temperatures might have different morphology and/or chemical structure which leads in turn to their differentiation in resistance to oxidation.

Table 3
Effect of DRM temperature on coke deposition onto Ni catalyst surface.

DRM temperature	Total amount of deposited carbon	
(°C)	(μmol)	(wt%)
500	128	1.0
600	1241	9.9
700	1129	9.0
800	886	7.0

Quantitative data for the total amount of carbon deposited onto the catalyst surface under steady-state conditions are summarized in table 3. The increase in temperature from 500 to 600 °C drastically accelerated the rate of coke deposition: one can see that the amount of carbon deposit increased by nearly an order of magnitude. It could be assigned to the changes occurring in the mechanism of carbon deposition. According to literature [22,23] and our calculations (table 4), at 500 °C the most thermodynamically favorable process leading to formation of coke is the Boudouard reaction (shown under number 1 in table 4) which is catalyzed by nickel. At 600 °C, the spontaneous dissociative adsorption of methane to carbon and hydrogen also becomes achievable and thus contributes to coke deposition (reaction (2) in table 4). However, it should be noted that a rise in reaction temperature further resulted in lowering the amount of de-

Table 4
Reactions involving carbon: free (Gibbs) energy values *vs.* reaction temperature.

Reaction	ΔG^0 (kJ) at temperature			
	500 °C	600 °C	700 °C	800 °C
(1) $2CO \rightleftharpoons C_{graphite} + CO_2$	−32.1	−12.9	6.3	25.8
(2) $CH_4 \rightleftharpoons C_{graphite} + 2H_2$	8.2	−1.0	−10.1	−19.1
(3) $C_{graphite} + H_2O_{gas} \rightleftharpoons CO + H_2$	21.6	5.8	−10.2	−26.5

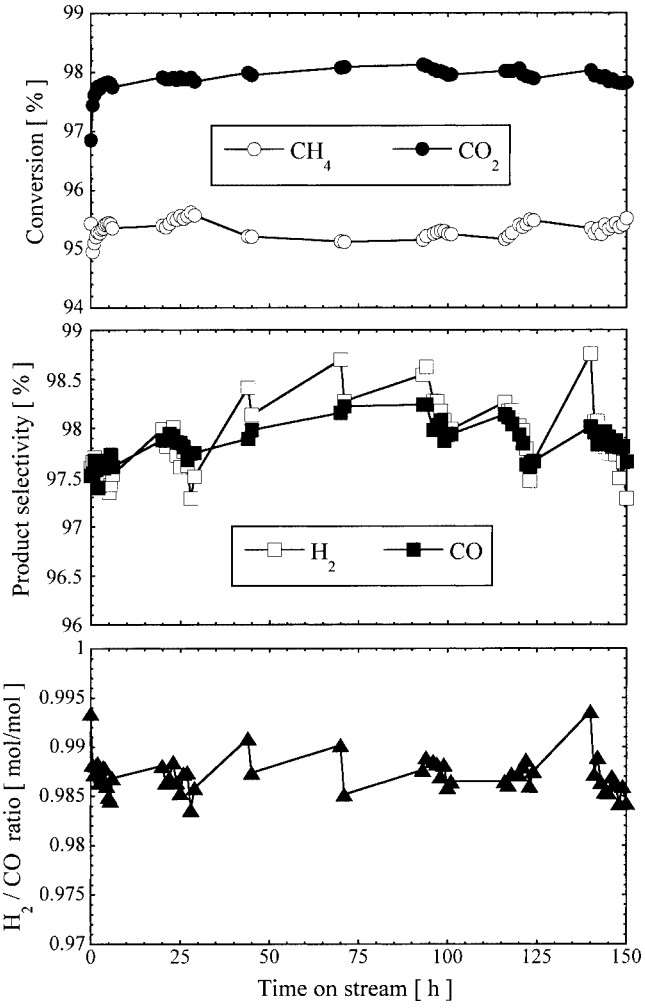

Figure 7. Check on the durability of Ni catalyst toward dry reforming of methane at 800 °C.

posited coke (table 3). This finding indicates that at higher temperature the carbon deposit appeared to become more reactive and could be gasified by water vapor (see reaction (3) in table 4) and by carbon dioxide (reversed Boudouard reaction), both reactions becoming spontaneous at temperature higher than 680 °C.

3.3. A check on the durability of Ni catalyst

As the Ni catalyst revealed no visible loss in activity within 6 h time on stream, it was worthwhile to examine its durability toward DRM reaction at 800 °C for longer time. Thus, the experiment with 150 h time on stream was carried out with pre-reduced catalyst. The results obtained for reagent conversion, product selectivity and H_2 to CO ratio as functions of time on stream are shown in figure 7. One can see that conversion of CH_4 and CO_2 remained as high as 95.5 and 98%, respectively. Selectivity to both H_2 and CO ranged within 1% from 97.5 to 98.5%. However, due to RWGS side reaction the H_2/CO ratio did not reach the unity value (though being as high as 0.985), and a trace amount of water vapor was always detected by GC in the post-reactor (effluent) gas stream.

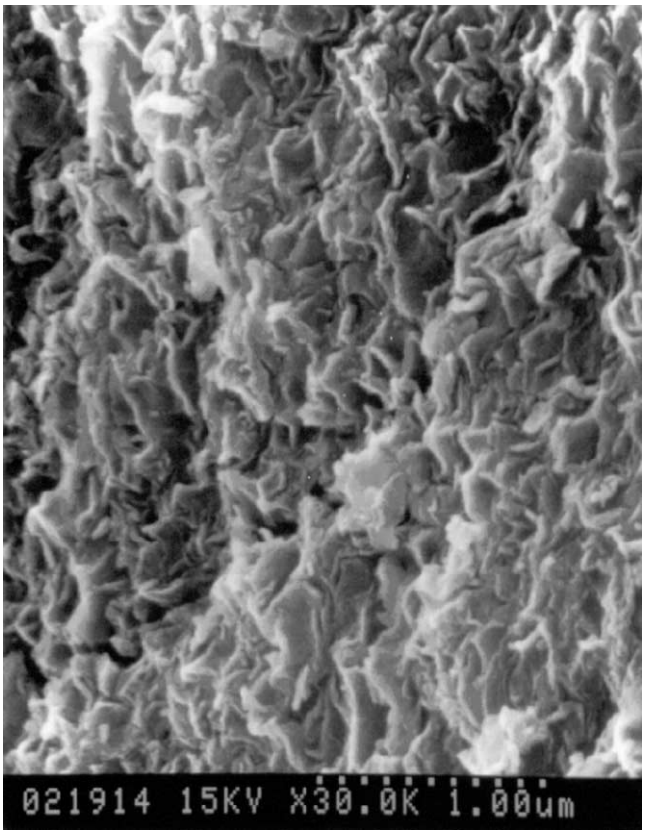

Figure 8. SEM image of the surface of reductively treated Ni catalyst (sample was not subjected to DRM reaction).

3.4. Morphology of catalytically produced carbon deposit

Surface morphology of the reductively treated (but not subjected to DRM) Ni catalyst can be evaluated from the SEM image in figure 8. It is seen that the catalyst surface resembled the agglomeration of flakes of irregular shape. However, after 150 h DRM run at 800 °C the surface of the catalyst completely changed. It became covered with carbon of various textures. Most part of the catalyst surface was coated with sponge-like carbon as it is seen in figure 9(A). Some amount of filamentous carbon was observed also (B). The least part of coke was presented with small agglomerates of separate carbon grains (C). Fine carbon filaments up to tens of μm in length were also observed (as it is shown in figure 9(C)) as well as carbon coils (D). The argument, confirming that most of deposited carbon was of graphite structure, came from TEM observations of the same spent catalyst

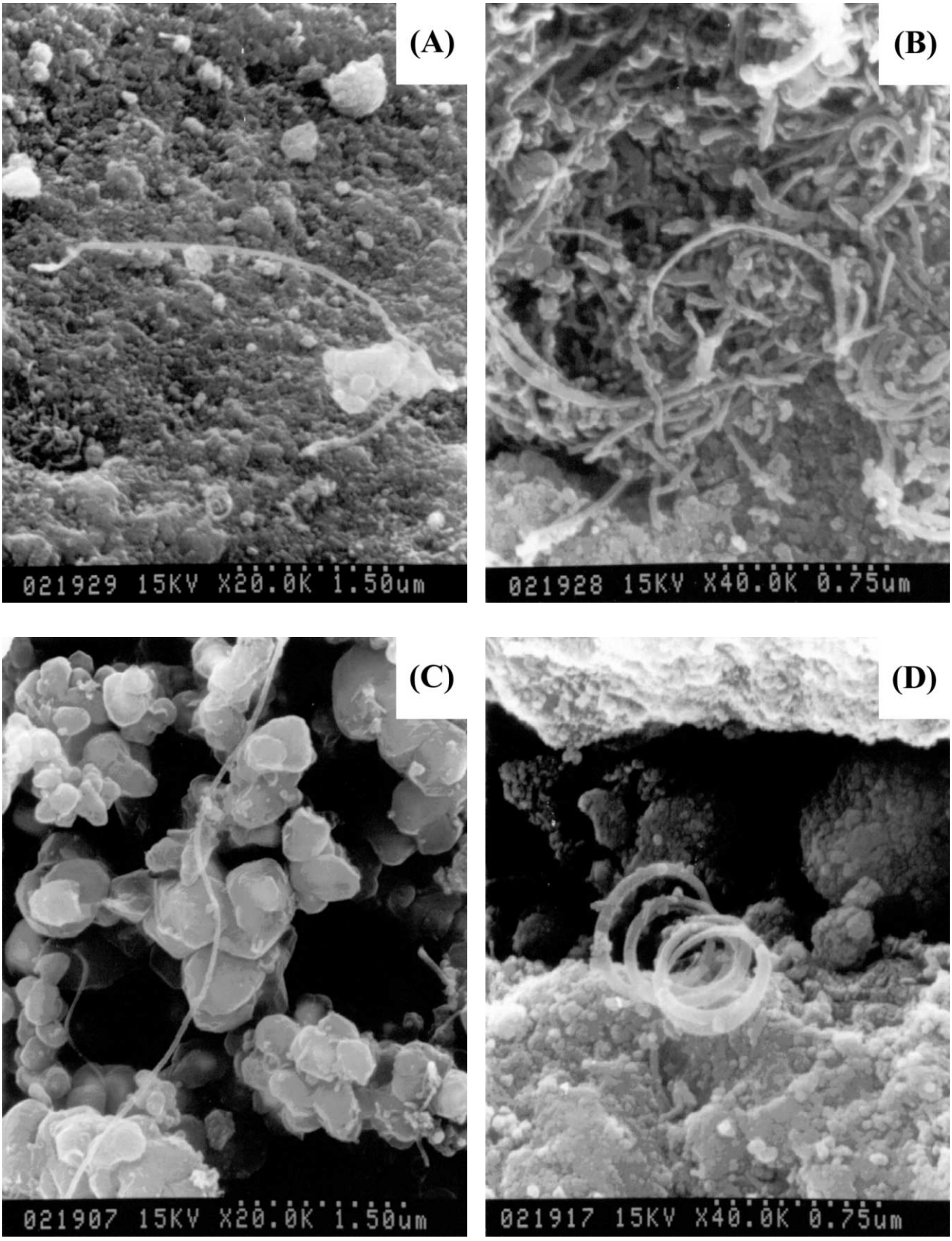

Figure 9. SEM images of Ni catalyst surface after 150 h DRM run at 800 °C.

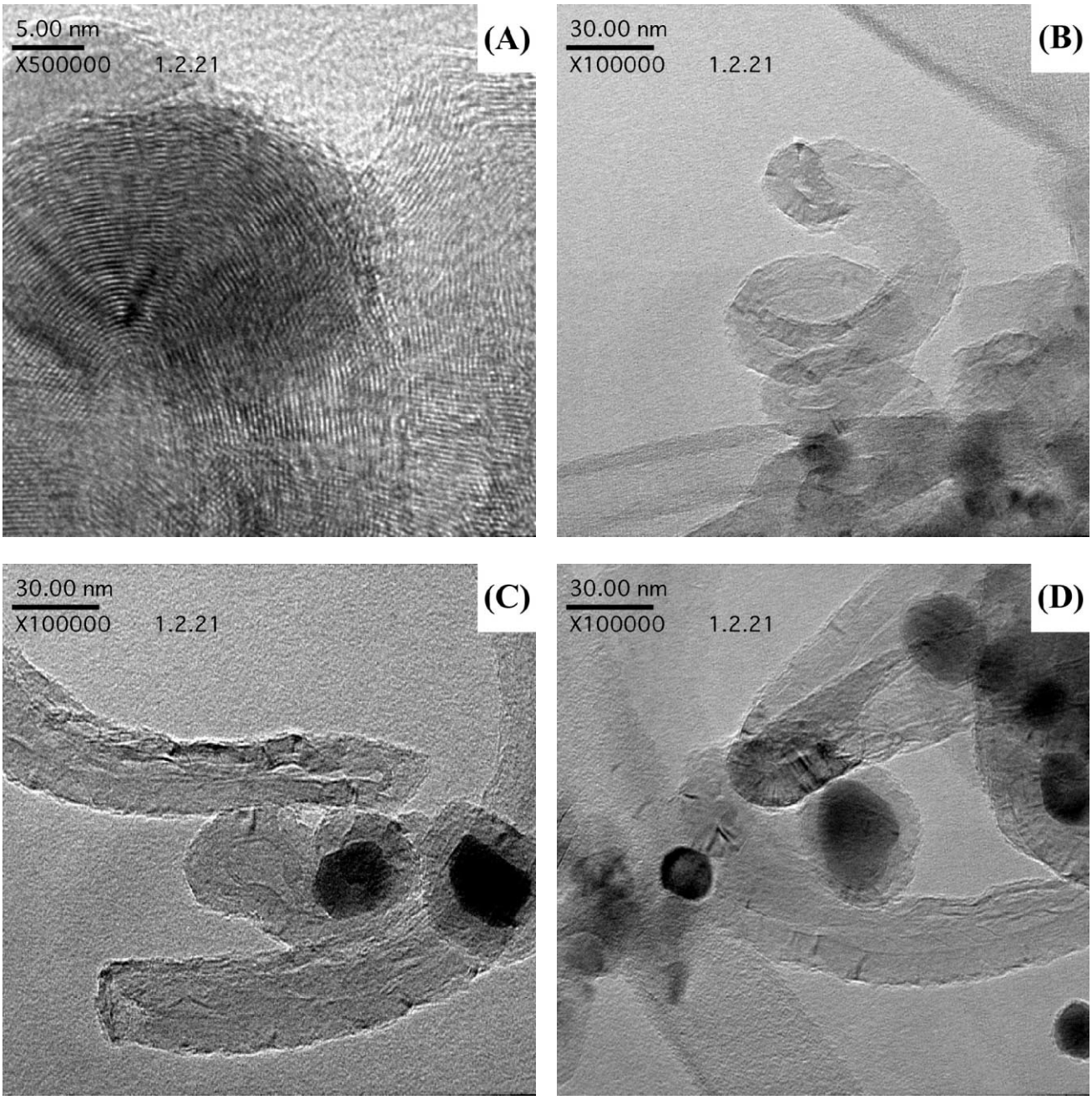

Figure 10. TEM micrographs of Ni catalyst after exposure to DRM reaction at 800 °C for 150 h.

(figure 10(A)). Carbon filaments and coils were also graphitic (B) and possessed with many surface defects. Nickel particles ranged in size from 15 to 35 nm and were mostly encapsulated with graphitic shells, as it is shown in figure 10(C). The smallest fraction of Ni particles remained uncovered with carbon even after 150 h DRM reaction (D).

3.5. A check on the reusability of Ni catalyst

The meaningful characteristic of a catalyst for practical application in industry is its suitable reusability. To check such a property of the Ni catalyst which was derived from MgAl–NiY LDH, three consecutive DRM trials were performed at 800 °C for 6 h, with TPO of deposited coke and subsequent reduction of the oxidized catalyst with hydrogen ($H_2 : N_2$ 10 : 35 $cm^3\,min^{-1}$) at 600 °C for 1 h after every DRM trial. The results obtained are shown in figure 11. As can be seen in this figure, conversion of CH_4 and CO_2 decreased by nearly 1% after the first DRM–TPO–reduction cycle, still being as high as 93.5 and 97%. The third DRM run revealed CH_4 and CO_2 conversion of the same values as of the second one. Additionally, for all three consecutive DRM trials the selectivity to H_2 and CO was as high as 97.5%.

The results of the temperature-programmed oxidation of deposited coke are shown in figure 12 and table 5. As it

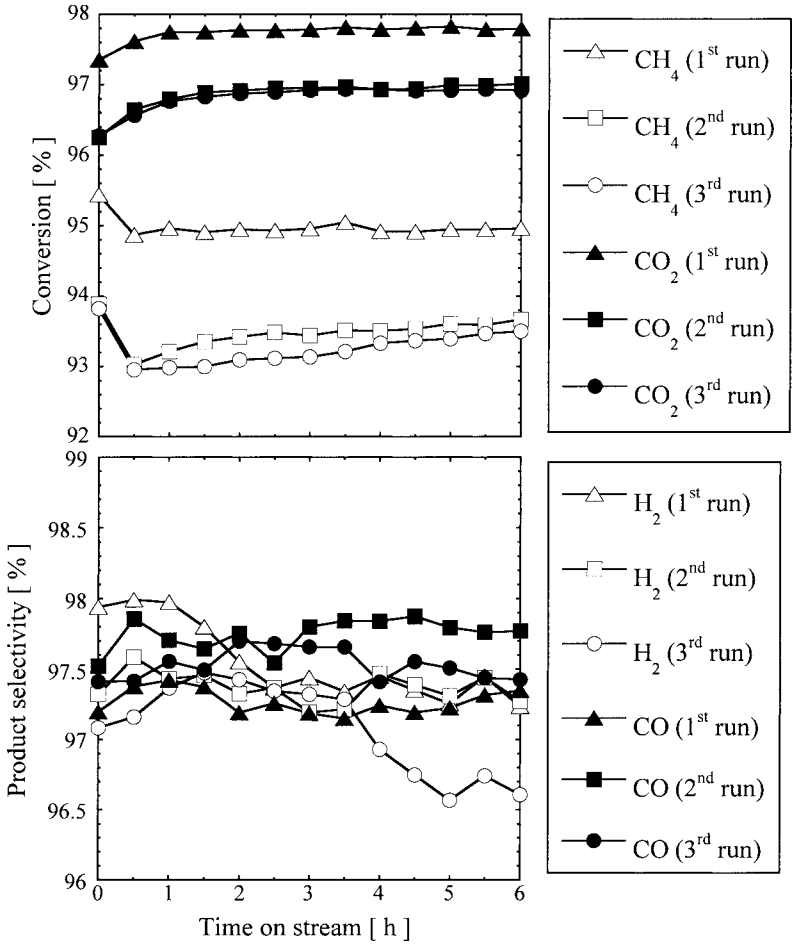

Figure 11. Check on the reusability of Ni catalyst derived from MgAl–NiY LDH.

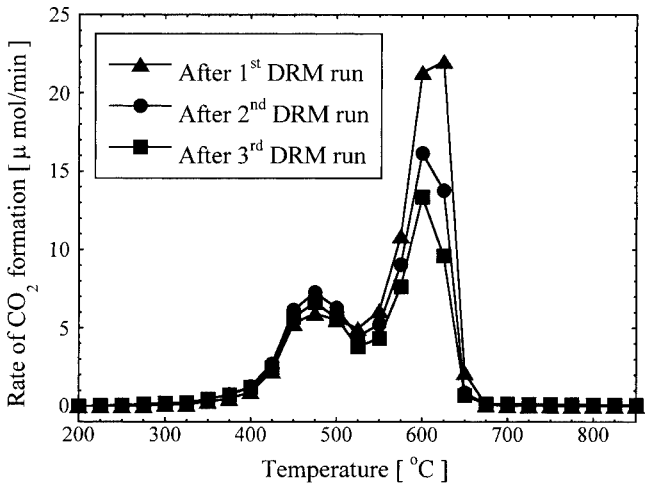

Figure 12. Temperature-programmed oxidation of coke deposited over Ni catalyst during consecutive DRM runs.

Table 5
Coke deposited over Ni catalyst during consecutive DRM runs.

Run number	Total amount of deposited carbon	
	(μmol)	(wt%)
1	886	7.0
2	762	6.1
3	641	5.1

is seen in figure 12, all three TPO "spectra" of CO_2 emission had two distinguishable peaks with maxima at 475 and 600–625 °C. Such observation indicated that, according to the number of peaks, consecutive DRM runs gave at least two kinds of carbon, differentiated by resistance to oxidation. An interesting feature can be drawn from the data in table 5: it is seen that the amount of deposited carbon decreased with increasing number of DRM trial. It could be attributed, for instance, to a decrease in surface area of catalytically active metallic nickel due to its sintering. Alternatively, under oxidative conditions of TPO nickel may "dissolve" in the mixed oxide support to form a NiO–MgO solid solution [24] which would cause the nickel content on the catalyst surface to diminish and therefore the coke formation rate to decrease.

4. Conclusion

It was shown that coprecipitation of Mg^{2+} and Al^{3+} with pre-formed NiY^{2-} species at a moderately high basic pH resulted in the formation of a novel LDH phase where NiY^{2-}

chelate resided within the interlayer space of Mg–Al layered double hydroxide. Incorporation of NiY^{2-} led to an increase in interlayer gallery distance to 9.9 Å compared with 3.0 Å of hydrotalcite. Intercalated NiY^{2-} species kept integrity as confirmed with results of DRIFT and TG-DTA studies.

Calcination of MgAl–NiY LDH at 500 °C and subsequent reduction with hydrogen afforded a new Ni catalyst suitable for reforming of methane with carbon dioxide to synthesis gas. Such a catalyst demonstrated an appropriate durability and could be used repeatedly after regeneration treatment. Although the amount of catalytically produced coke attained up to 10 wt%, the coke deposition did not cause a deactivation of the catalyst: both conversion of reagents and product selectivity remained high and stable since zero value of time on stream. It suggested that under steady-state conditions the catalytically produced coke was not inert and could be gasified by CO_2 and by steam.

The high catalytic performance of the system reported in this work should be attributed not only to a new Ni catalyst but also to a reaction design. The upstream feed of reagent gases caused the catalyst to "boil" and therefore provided the fluidized-bed condition for the catalyst rather than the fixed-bed one. It allowed avoiding such drawbacks of the fixed-bed catalytic reactor as its clogging and inhomogeneous distribution of heat in the catalyst bed (*i.e.*, "hot spot" effect).

In our future studies, catalytic properties of the reported Ni catalyst will be explored more in detail and be compared with those of catalysts prepared by other techniques. Research on factors affecting the carbon deposition onto the catalyst surface is also in progress.

Acknowledgement

The support of this work by the New Energy and Industrial Technology Development Organization (NEDO) is gratefully acknowledged. The authors would like to thank Drs. Kunio Uchida and Tatsuo Tsunoda for assistance with SEM and TEM studies, Dr. Hideo Orita for valuable comments on DRIFT results and Mami Nabeshima for her help with ICP-ES measurements.

References

[1] M.C.J. Bradford and M.A. Vannice, Catal. Rev. Sci. Eng. 41 (1999) 1.
[2] S. Wang and G.Q. Lu, Appl. Catal. A 169 (1998) 271.
[3] S. Tang, L. Ji, J. Lin, H.C. Zeng, K.L. Tan and K. Li, J. Catal. 194 (2000) 424.
[4] T. Hayakawa, S. Suzuki, J. Nakamura, T. Uchijima, S. Hamakawa, K. Suzuki, T. Shishido and K. Takehira, Appl. Catal. A 183 (1999) 273.
[5] Y.H. Hu and E. Ruckenstein, Catal. Lett. 36 (1996) 145.
[6] Y.H. Hu and E. Ruckenstein, Catal. Lett. 43 (1997) 71.
[7] E. Ruckenstein and Y.H. Hu, Appl. Catal. A 154 (1997) 185.
[8] E. Ruckenstein and Y.H. Hu, Catal Lett. 51 (1998) 183.
[9] K. Tomishige, Y.-G. Chen and K. Fujimoto, J. Catal. 181 (1999) 91.
[10] Y.-G. Chen, K. Tomishige, K. Yokoyama and K. Fujimoto, J. Catal. 184 (1999) 479.
[11] US Patent 5 767 040 (1998).
[12] F. Cavani, F. Trifirò and A. Vaccari, Catal. Today 11 (1991) 173.
[13] A.I. Tsyganok, K. Suzuki, S. Hamakawa, K. Takehira and T. Hayakawa, Chem. Lett. (2001) 24.
[14] A. Vaccari, Catal. Today 41 (1998) 53.
[15] V. Rives and S. Kannan, J. Mater. Chem. 10 (2000) 489.
[16] J.R. Hart, in: *Ullmann's Encyclopedia of Industrial Chemistry*, Vol. A10, eds. W. Gerhartz and Y.S. Yamamoto (VCH, Weinheim, 1987) pp. 95–100.
[17] US Patent 2 387 735 (1945).
[18] US Patent 3 061 628 (1962).
[19] K. Nakamoto, *Infrared and Raman Spectra of Inorganic and Coordination Compounds*, Part B: Applications in Coordination, Organometallic, and Bioinorganic Chemistry (Wiley–Interscience, New York, 1997) ch. III-9.
[20] F.L. Garvan, in: *Chelating Agents and Metal Chelates*, eds. F.P. Dwyer and D.P. Mellor (Academic Press, New York, 1964) ch. 7.
[21] K. Nakamoto, *Infrared and Raman Spectra of Inorganic and Coordination Compounds*, Part A: Theory and Applications in Inorganic Chemistry (Wiley–Interscience, New York, 1997) ch. I-18.
[22] J.B. Claridge, M.L.H. Green, S.C. Tsang, A.P.E. York, A.T. Ashcroft and P.D. Battle, Catal. Lett. 22 (1993) 299.
[23] G.A. Somorjai, *Introduction to Surface Chemistry and Catalysis* (Wiley–Interscience, New York, 1994) p. 489.
[24] F. Arena, F. Frusteri, A. Parmaliana, L. Plyasova and A.N. Shmakov, J. Chem. Soc. Faraday Trans. 92 (1996) 469.